Thickness-Controlled *Quasi*-Two-Dimensional Colloidal PbSe Nanoplatelets

Weon-kyu Koh[†⊥], Naveen K. Dandu[‡⊥], Andrew F. Fidler[†], Victor I. Klimov[†], Jeffrey M. Pietryga[†*], and Svetlana V. Kilina[‡*]

[†]Center for Advanced Solar Photophysics, C-PCS, Chemistry Division, Los Alamos National Laboratory, Los Alamos, New Mexico 87545, United States

[‡]Department of Chemistry and Biochemistry, North Dakota State University, Fargo, North Dakota 58108, United States

[⊥]These authors contributed equally.

* Corresponding author email: pietryga@lanl.gov; svetlana.kilina@ndsu.edu

Supporting Information

Table of Contents

S1. Synthesis and Physical Characterization of PbSe NPLs

General Considerations. All syntheses were performed under exclusion of air and moisture using standard Schlenk or inert-atmosphere glovebox techniques. Lead (II) chloride ($PbCl_2$, Alfa Aesar, 99.999%), lead (II) bromide (Alfa Aesar, 99.999%), lead (II) iodide (Sigma Aldrich, 99.999%), selenium powder (Sigma Aldrich, 99.999%), oleic acid (Sigma Aldrich, 90%), oleylamine (Acros, 80-90%), n-octylamine (Fisher Scientific, 99+%), Aliquat 336 (Acros), ethanol (Sigma Aldrich, pure anhydrous), and chloroform (Sigma Aldrich, anhydrous) were used without further purification.

Synthesis of PbSe NPLs. 0.4 mmol of $PbCl_2$ is mixed with 2.5 ml of oleylamine, 2.5 ml of octylamine, and 2 mmol of Aliquat 336, and heated to 120 ºC under flowing inert atmosphere for 30 min to remove air and water. After cooling to 50 ºC, 2 mmol of Se powder in a mixture of 1.3 ml of octylamine and 1.3 mL of oleylamine is injected, and the mixture is stirred for 20 min. The product is precipitated by adding excess ethanol, and after centrifugation and decanting of the supernatant, is then redispersed in chloroform. Repeated precipitation and redispersion allows for more complete removal of residual reactants. To prevent aggregation, 1 mL of oleic acid can be added prior to the addition of ethanol for each precipitation step. For NPLs of larger thicknesses, the $PbCl_2$ was replaced by an equimolar amount of PbI_2, and the reaction was allowed to proceed for up to 3 h. Increasing the reaction temperature up to 100 ºC has no evident effect on the $PbCl_2$-based reaction; in the case of PbI_2, the progressive thickening occurs more quickly (e.g., conversion of 2 nm NPLs to 4 nm NPLs takes <10 min, as opposed to ~90 min).

Characterization. Transmission electron microscope (TEM) images were taken of samples drop-cast onto carbon-coated grids using a JEOL 2010 TEM. Optical absorption spectra were measured using a Perkin Elmer Lambda 950 spectrophotometer. Photoluminescence (PL) spectra were collected from chloroform solutions of NPLs, using 808 nm excitation from a diode laser, and a LN2-cooled InSb detector with a grating monochromator. The excitation was mechanically chopped, and the signal was enhanced by a lock-in amplifier. PL quantum yields were estimated by comparison to the integrated intensity of a IR-26 standard (solution in 1,1-dichloroethane) after adjusting for difference in optical density at 808 nm. Ensemble NPL thickness for each sample was determined by small-angle X-ray scattering, which was carried out using a Rigaku

Utima III diffractometer (Cu Kα radiation). The atomic ratios of Pb to Se were determined by elemental analysis using a Shimadzu ICPE-9000 inductively-coupled plasma atomic emission spectrometer (ICP-AES).

Table S1. Elemental analysis for PbSe NPLs measured by ICP-AES. Compared to literature values for PbS and PbSe quantum dots (QDs) with diameters similar to these thicknesses,[1] the Pb:Se ratio for PbSe NPLs is generally closer to unity. This likely reflects the increased dominance of the stoichiometric (100) faces.

NPL thickness	Pb:Se	Standard deviation	Pb:Se for QD
2.1 nm	1.32:1	0.08	2:1
4.2 nm	1.13:1	0.11	1.5:1
6.3 nm	1.01:1	0.07	1.3:1

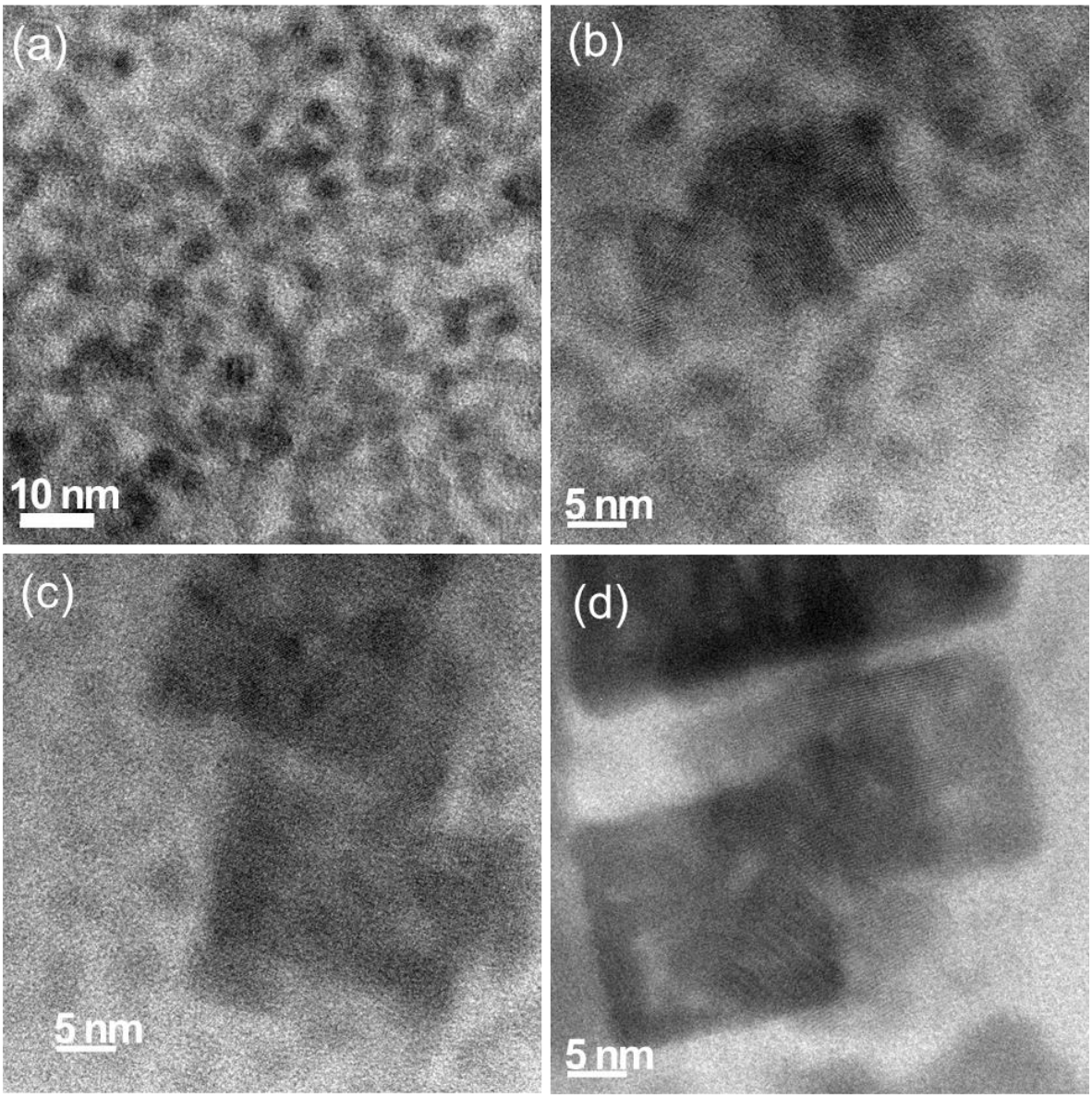

Figure S1. TEM images of the product of a $PbCl_2$-based PbSe NPL synthesis (50 °C) at: (a) 2 min; (b) 5 min; (c) 10 min; and (d) 20 min.

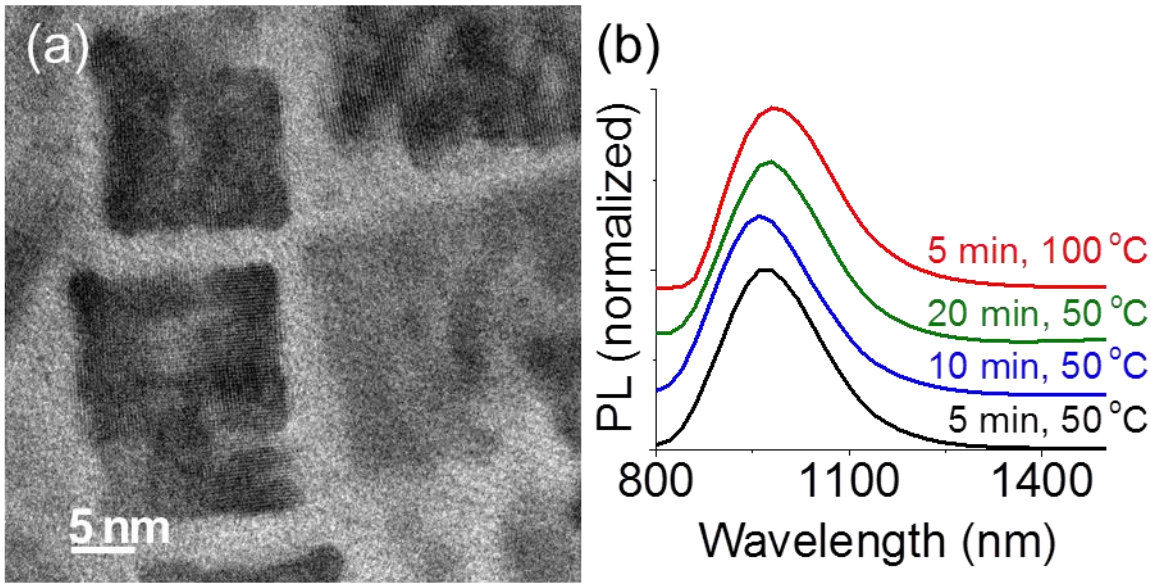

Figure S2. (a) TEM images of Pb Br_2-based PbSe NPLs. (b) PL spectra of $PbBr_2$-based PbSe NPLs stay relatively constant regardless of reaction time, even if temperature is elevated.

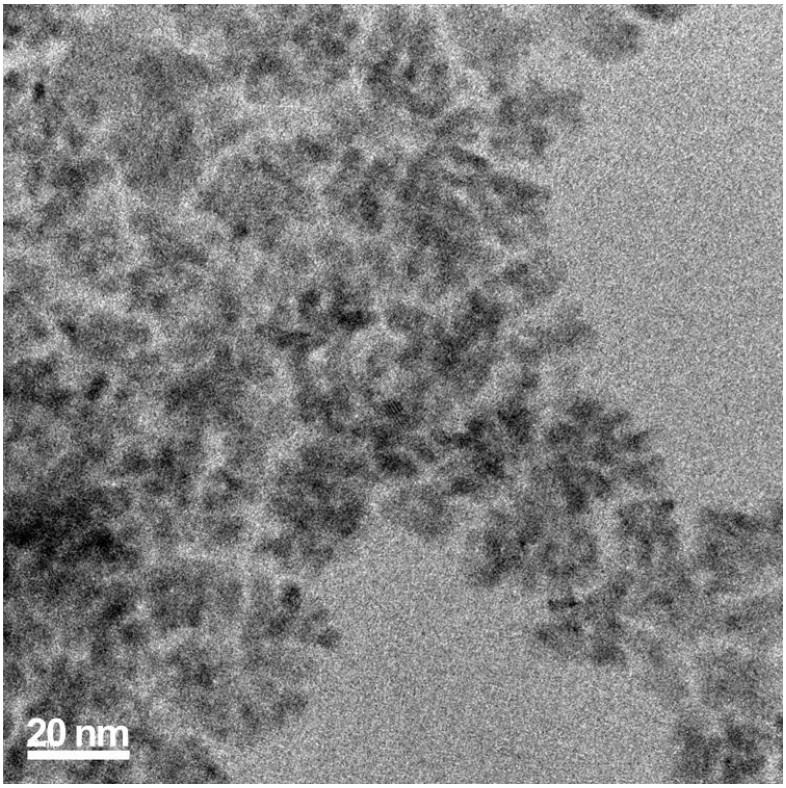

Figure S3. TEM image of the product of a PbI_2 reaction without an added source of Cl^- after 20 min. Small QDs form and begin to form clusters, but without distinct shape.

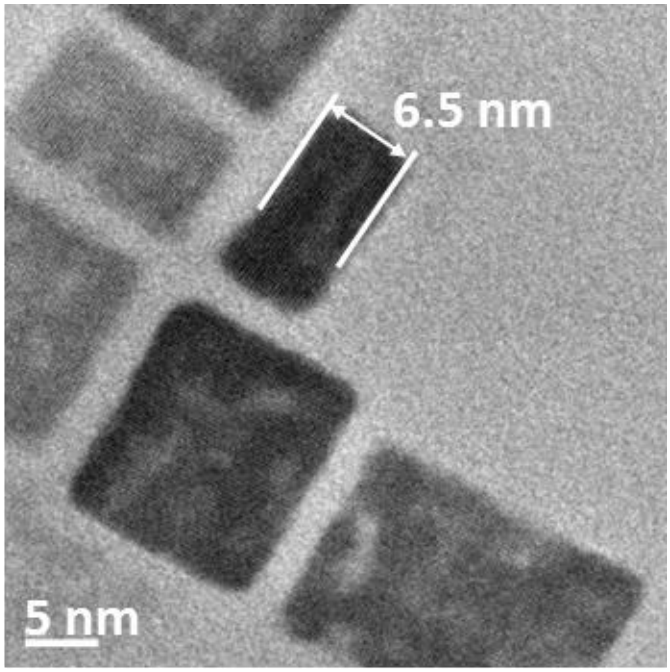

Figure S4. TEM of a sample of thick NPLs produced after longer reaction times with PbI_2. The highlighted NPL is oriented edge-on, showing its thickness.

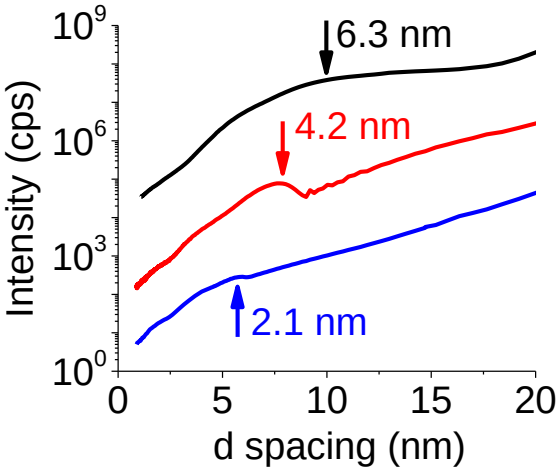

Figure S5. SAXS patterns of PbSe NPL samples, with extracted thicknesses after accounting for a ligand bilayer.

S2. Computational Details

S2.1. Gaussian calculations of surface-dependent ligand binding and bridge formation:

The quantum dots (QDs) we simulated are $Pb_{16}Se_{16}$ and $Pb_{68}Se_{68}$ clusters with diameters of about 1 nm and 1.8 nm, respectively, constructed based on a rock-salt lattice with bulk Pb-Se bonds, as described elsewhere.[2] The Cl^-, $PbCl_2$, and amine (as CH_3NH_2) ligands are initially placed at the (100), (111), or (110) surfaces at distances typical for Pb-Cl and Pb-N bond lengths. All structures are then optimized to their lowest-energy configurations using the Gaussian-09[3] suite of quantum chemical programs. We have utilized PBE1PBE[4] functional with LANL2DZ[5] basis set for heavier atoms (Pb, Se, I), and 6-31G*[6] for the rest of the atoms. In addition to energetically optimized vacuum calculations, the resulting geometries of several selected systems were also optimized in propylamine solvent, to reflect the typical reaction medium of experimental studies. Solvent effects were simulated using the conductor-like polarizable continuum model (CPCM)[7] with the appropriate dielectric constant, as incorporated in the Gaussian-09 software package. The QD-ligand binding energies (per ligand) are calculated as the energy difference between the QD functionalized by the particular ligands and the isolated QD and ligand, and then divided by the number of ligands passivating the surface. Each structure used for the binding energy calculations is, again, optimized in propylamine solvent. A generalized scheme describing different surfaces on PbSe quantum dot is shown in the main text in Figure 2a. Our QDs comprise 6 surfaces in the (100), 12 surfaces in the (110), 8 surfaces (4 lead-terminated and 4 selenium-terminated) in the (111) directions, respectively.

As represented in Figure 2b and Table S2, our calculations show that single Pb^{2+}, Cl^-, I^-, $PbCl_2$ and PbI_2 ligands bind significantly more strongly to (111) and (110) sites than to (100) sites, with Pb^{2+} yielding the strongest binding. To check whether this result is affected by high concentrations of ligands, such as under experimental conditions, we simulated each surface with more ligands attached (Figure 2c and Table S3). As soon as the ligand coverage increased, we saw destabilization in the binding of charged ligands (Pb^{2+}, I^- and Cl^-), especially for (111) and (110) surfaces. In contrast, the binding energy remained nearly unchanged in the case of neutral PbX_2 (X = Cl or I) ligands. This suggests that (110) and (111) surfaces are likely passivated primarily by PbX_2 ligands, either directly attaching from solution, or formed from the binding of negatively charged Cl^- and I^- ions to individual Pb^{2+} ions already bound to the surface.

Table S2. The binding energies between the charged and neutral ligands and each of three surfaces of the $(PbSe)_{68}$ QDs calculated in propylamine solvent.

Ligand attachment face on $(PbSe)_{68}$	Binding energy per ligand (eV)					
	Cl^-	I^-	Pb^{2+}	$PbCl_2$	PbI_2	NH_2Me
100	-0.8	-0.54	-4.57	-1.91	-1.75	-0.79
110	-1.06	-0.89	-5.72	-2.18	-2.11	-0.53
111	-1.25	-1.09	-5.72	-1.77	-1.79	-0.43

Table S3. The calculated binding energies between the charged and neutral ligands and each of three surfaces of the $(PbSe)_{68}$ QDs for a various number of ligands attached. Calculations are done in propylamine solvent.

Ligand attachment face on $(PbSe)_{68}$	Number of ligands attached	Binding energy per ligand (eV)				
		Cl^-	I^-	Pb^{2+}	$PbCl_2$	PbI_2
100	1	-0.94	-0.54	-4.57	-1.91	-1.75
	2	-0.80	-0.40	-4.01	-1.89	-1.73
	4	-0.98	-0.71	-1.71	-1.85	-1.55
110	1	-1.20	-0.89	-5.72	-2.18	-2.11
	2	-1.06	-0.76	-5.19	-2.17	-2.09
	4	-0.66	-0.41	-3.51	-2.06	-1.95
111	1	-1.40	-1.09	-5.72	-1.77	-1.79
	2	-1.25	-0.85	-5.10	-1.74	-1.75
	4	-0.82	-0.53	-3.72	-2.16	-2.07

In contrast, we found that amines preferentially bind to (100) sites over both (110) and (111), although both the surface-dependence and the overall binding strengths are substantially weaker than for other ligands (Figure 2b and Table S2). The weaker QD-amine interactions allow us to assume that amine ligands can be easily shifted from one surface to another or completely exchanged by other ligands. In fact, amines initially placed at the (110) surface, or at the edge of (111)/(110) surfaces of $(PbSe)_{16}$ are pushed to the (100) surface by $PbCl_2$ upon geometry optimization, leaving $PbCl_2$ strongly bound to the (110) side, as shown in Figure S5c.

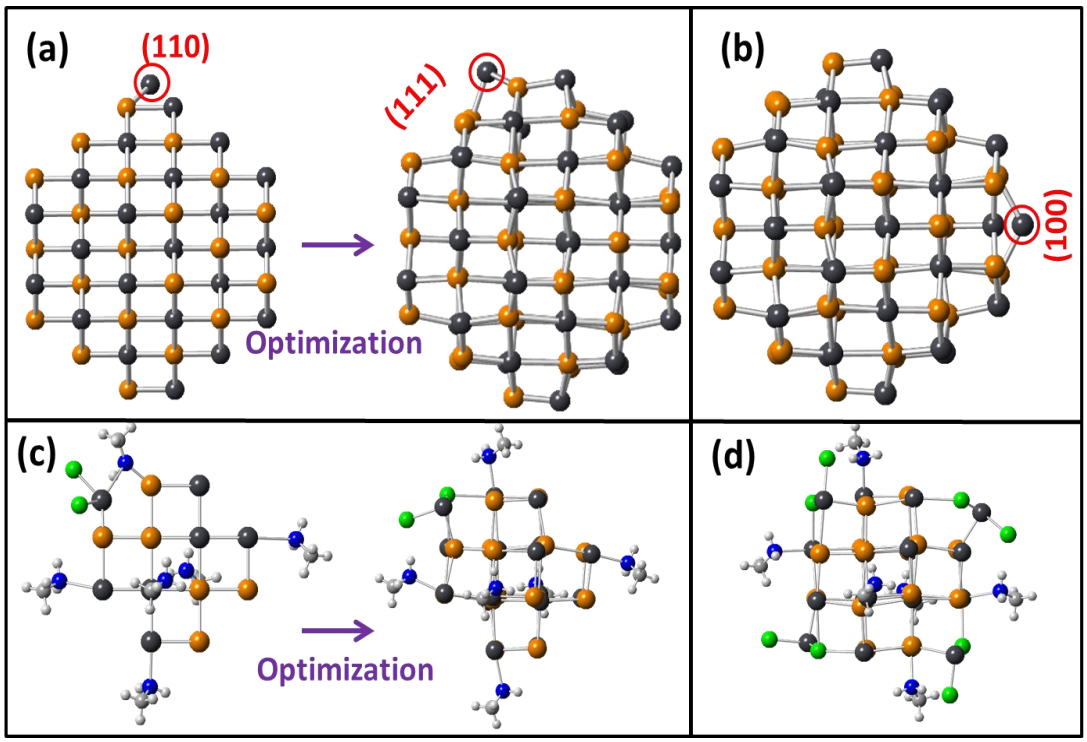

Figure S6: (a and b) Calculated structures of a $Pb_{68}Se_{68}$ QD of 2 nm diameter with an adsorbed Pb^{2+} ion on (110), (111) and (100) faces. (c) The most stable fully passivated $Pb_{16}Se_{16}$ with 6 NH_2Me ligands on the (100) and four $PbCl_2$ on the (110) surfaces (d).

Because binding of amines to QD surfaces is relatively weak, it is easily conceivable that random collisions between QDs might provide enough energy to detach amines from the surface, leaving the (100) surface deficient in ligand coverage. This is important for two QDs to be able to join at opposing (100) surfaces. A key feature of these QDs that promotes this surface-specific fusion are the $PbCl_2$ ligands at the (110) and (111) surfaces, which possess Pb-Cl bond lengths that are ideal for forming bridging interactions between QDs (Figure S6).

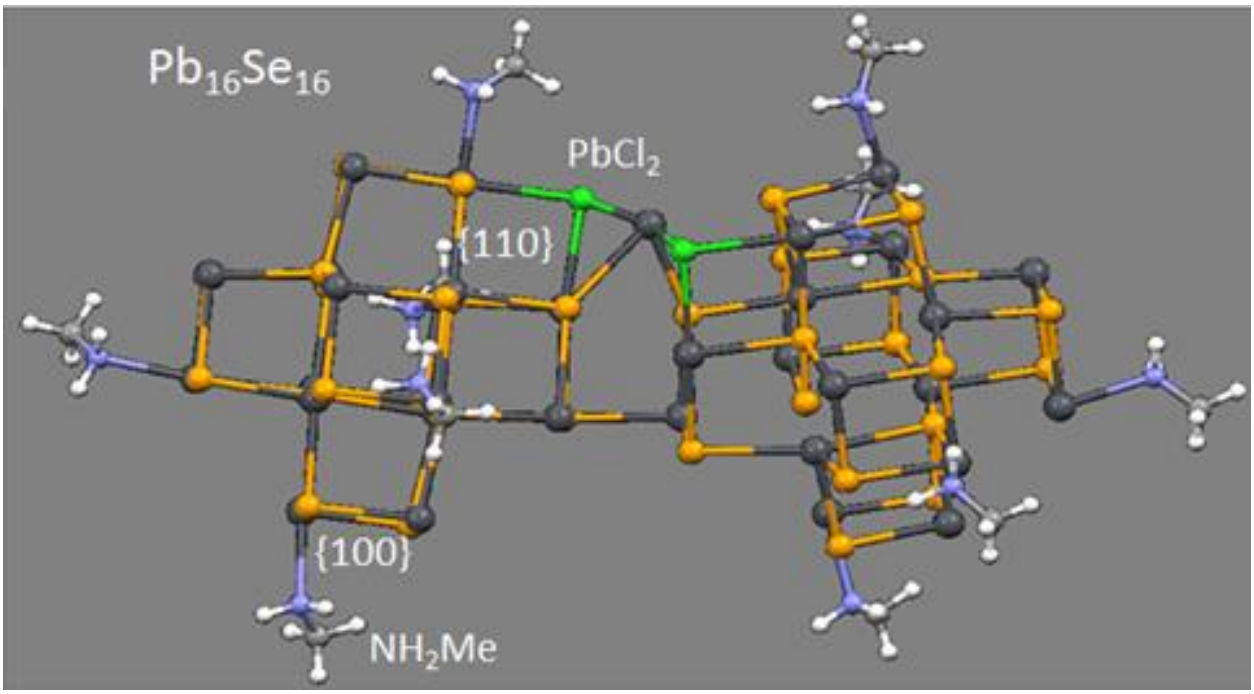

Figure S7: Gaussian simulations of two PbSe QDs passivated with amines on 5 different (100) sites and $PbCl_2$ on (110). After relaxation, $PbCl_2$ at (110) tend to form a bridge between two QDs.

S2.2 VASP calculations of NPL surface energies.

To examine the attachment process in more detail, we performed calculations using the VASP code[8] and simulated periodic boundary conditions to mimic QDs growing in 2D and 3D directions. Explicitly, we have utilized the Perdew, Burke and Ernzerhof (PBE) functional[4a,9] and plane-wave basis sets[10] within PAW pseudopotentials for these calculations. Periodic boundary conditions (PBC) were applied between the quantum dots to form 0-, 2- and 3-dimensional structures. In the modeling, 0D $(PbSe)_{68}$ QDs are surrounded by vacuum of about 10 Å in all three directions, thus excluding spurious interactions between their periodic images. 2D structures were obtained by applying PBC in such a way that each QD is one Pb-Se bond length (~2.9 Å) apart from each other in 2 directions, with 18 Å of vacuum in the third direction; in 3D structures, the PBC is applied such that each QD is 2.9 Å apart in all directions. Electronic relaxations were performed until a threshold of 10^{-5} eV was reached while the ionic relaxations were performed until a threshold of 10^{-2} eV/Å was reached and energy cutoff of 300 eV was set

in each of these calculations. A mesh of 6x6x6 and 6x6x1 Monkhorst-Pack grid[11] was used to sample the Brillouin zone in 3D and 2D cases, respectively. Gamma-point calculations were done for 0D QDs.

Calculations of the surface energy. We use the example of $(PbSe)_{68}$ passivated by 12 of $PbCl_2$ ligands at (110) sites to illustrate how to calculate the surface energy of QDs in the presence of ligands. The surface energy $\gamma_{110}^{\text{bare}}$denotes the relative stability of the (110) surfaces of bare $(PbSe)_{68}$ QDs, which can be calculated using eq-1 as follows:

$$\gamma_{110}^{bare} = \frac{1}{12\,A_{110}}(E_{0D/bare} - 24E_{Pb} - 24E_{Se}) \quad (1)$$

Here, the number 12 represents the number of (110) surfaces per $Pb_{68}Se_{68}$ QD; A_{110} is the surface area of each; $E_{0D/bare}$, E_{Pb} and E_{Se} represent the energy of the optimized bare QD, the energy of isolated lead atom and the energy of isolated Se atom, respectively. As shown in Figure 2a, each (110) surface contains 2 Pb atoms and 2 Se atoms: thus, a total of 24 Pb and 24 Se atoms are involved in binding with ligands.

Below, we describe how we derive the surface energies of more complex structures involving attachment of QDs and various ligand coverages. The surface energy associated with the formation of a 2D plate constructed of $(PbSe)_{68}$ QDs along the (100) direction, passivated by $PbCl_2$ at 110 sites, denoted by $\gamma_{PbCl_2}^{2D}$, can be calculated as follows:

$$\gamma_{PbCl_2}^{2D} = \frac{1}{4\,A_{100}}(E_{2D/(QD-PbCl_2)} - 32E_{Pb} - 24E_{Se} - 16E_{Cl}) \quad (2)$$

where the number '4' reflects attachment in x, x', y and y' directions, $E_{2D/(QD\text{-}PbCl2)}$ is the energy of 2D plate growing along x, x', y and y', constructed by attachment of $PbCl_2$ at the (110) surface, and E_{Cl} is the energy of isolated Cl atom, respectively. As seen in Figure S7, each of (100) surfaces contains 6 Pb atoms and 6 Se atoms from the QD itself, along with 4 Pb atoms and 8 Cl atoms from the (110) associated $PbCl_2$ ligands. For

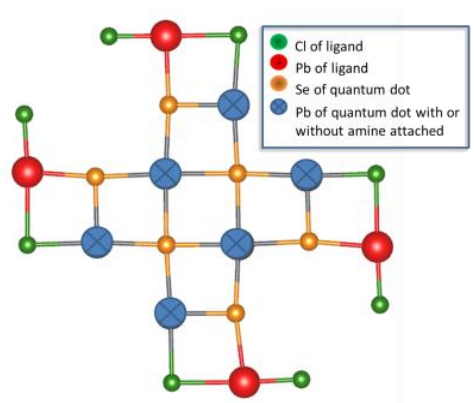

Figure S8: 100 surface of $(PbSe)_{68}$ quantum dot with 12 $PbCl_2$ on 110 surfaces growing in x, x', y and y'

the 4 surfaces, a total of 8 * 4 = 32 Pb (6 Pb from the QD, 4 Pb from ligand, which is shared with an adjacent dot, so 4 /2 = 2 Pb), 24 Se and 16 Cl atoms are involved in 2D plate formation.

Surface energy for the formation of the 3D attachment structure constructed of $(PbSe)_{68}$ QDs along the (100) direction, passivated by $PbCl_2$ at 110 sites, can be calculated as follows:

$$\gamma_{PbCl_2}^{3D} = \frac{1}{2\,(A_{xy}+A_{yz}+A_{zx})_{100}}\left(E_{3D/(QD-PbCl_2)} - 48E_{Pb} - 36E_{Se} - 24E_{Cl}\right) \quad (3)$$

where '$2(A_{xy} + A_{yz} + A_{zx})$' represents the surface area of the structure resulting from a QD covered in all six directions, and $E_{3D/(QD\text{-}PbCl2)}$ is the energy of the 3D structure. By the arguments of the previous paragraph (Figure S7), for the 6 surfaces, a total of 8 * 6 = 48 Pb, 36 Se and 24 Cl atoms are involved in 3D structure formation.

To calculate the surface energy associated with amines attached to the (100) surface, we use the expression:

$$\gamma_{100}^{amines} = \frac{1}{2\,A_{100}}\left(E_{0D/QD-PbCl_2} - 20E_{Pb} - 12E_{Se} - 16E_{Cl}\right) \quad (4)$$

where, $E_{0D/QD-PbCl_2}$ is the energy of a QD covered with $PbCl_2$ at 110. The factor '2' represents that amines cover on 2 opposing surfaces, which according to the arguments of the preceding paragraphs, involve a total of 20 Pb, 12 Se and 16 Cl atoms.

Surface energy for the formation of a 2D plate of $(PbSe)_{68}$ quantum dot along 4 (100) surfaces, passivated by $PbCl_2$ at 110 sites and 2 CH_3NH_2 ligands on each side of the remaining (100) surfaces can be calculated as follows:

$$\gamma_{PbCl_2+\,CH_3NH_2}^{2D} = \frac{1}{4\,A_{100}}\left(E_{2D/(QD-PbCl_2-CH_3NH_2)} - 32E_{Pb} - 24E_{Se} - 16E_{Cl}\right) \quad (5)$$

where '4' represents the QD growing in four directions, $E_{2D/(QD\text{-}PbCl2\text{-}CH3NH2)}$ is the energy of the corresponding 2D plate constructed of PbSe QDs. For the 4 bonding surfaces, a total of 32 Pb, 24 Se and 16 Cl atoms are involved in 2D plate formation. It is important to note that all of the atom numbers in Eqs 1-5 will vary according to the size of quantum dot used.

The total adsorption energy of $PbCl_2$ on a 2D plate can be expressed as:

$$\Delta G^{2D}_{PbCl_2} = E_{2D/(QD-PbCl_2)} - E_{2D/bare} - 12E_{PbCl_2} \quad (6)$$

The total adsorption energy of $PbCl_2$ on a 3D structure can be expressed as:

$$\Delta G^{3D}_{PbCl_2} = E_{3D/(QD-PbCl_2)} - E_{3D/bare} - 12E_{PbCl_2} \quad (7)$$

The total adsorption energy of amines on a 2D plate can be expressed as:

$$\Delta G^{2D}_{PbCl_2+\,CH_3NH_2} = E_{2D/(QD-PbCl_2-CH_3NH_2)} - E_{2D/(QD-PbCl_2)} - 12E_{CH_3NH_2} \quad (8)$$

Total surface energy of 2D plate of $(PbSe)_{68}$ covered with $12PbCl_2$ growing in 4 directions of 100 is given by:

$$\Delta G^{2D} = \gamma^{bare}_{110} + \gamma^{2D}_{PbCl_2} + \frac{1}{4A_{100}} * \Delta G^{2D}_{PbCl_2} \quad (9)$$

Total surface energy of 3D box of $(PbSe)_{68}$ covered with $12PbCl_2$ growing in all 6 directions of 100 is given by:

$$\Delta G^{3D} = \gamma^{bare}_{110} + \gamma^{3D}_{PbCl_2} + \frac{1}{2\,(A_{xy}+A_{yz}+A_{zx})_{100}} * \Delta G^{3D}_{PbCl_2} \quad (10)$$

Total surface energy of 2D plate of $(PbSe)_{68}$ covered with 2 of amines on each of two 100 surfaces and $12PbCl_2$, growing in 4 directions of 100 is given by:

$$\Delta G^{2D(CH_3NH_2)} = (\gamma^{bare}_{110}) + (\gamma^{2D}_{PbCl_2+\,CH_3NH_2}) + (\gamma^{amines}_{100}) + \frac{1}{4A_{100}} * (\Delta G^{2D}_{PbCl_2+\,CH_3NH_2}) \quad (11)$$

2D vs. 3D attachment. Our simulation started by allowing a $(PbSe)_{68}$ QD with $PbCl_2$ ligands attached to each of the 12 (110) surfaces (Figure S7), surrounded in all (100) directions (x, y, z) with 18 Å of vacuum, to relax. We then simulated attachment in two dimensions by placing these QDs next to each other with a separation of roughly one Pb-Se bond length in two of the available (100) directions (Figure 3a). After relaxation, we observed that chlorides from the ligands served as bridges between the QDs, leading to the formation of plates, as shown in

Figure 3b. Similar behavior was seen when QDs were placed in all three dimensions, leading to 3D attachment.

To mimic the observation we made from our previous results from Gaussian calculations that amines are likely to passivate the (100) surface, we performed the simulation for 2D case again, but this time adding passivating amines (CH_3NH_2) at the top and bottom (100) surfaces that are not involved in the 2D interaction between the QDs. We then calculated surface energy changes associated with the formation of 2D and 3D structures.[12] From Figure 3d and Tables S4 and S5, it is clear that formation of 2D NPLs is more favorable than formation of 3D attachment structures. Similar behavior is observed when only 4 of (110) surfaces were passivated with $PbCl_2$. As the binding energy of $PbCl_2$ is similar in both (110) and (111) surfaces, we simulated NPL growth with $PbCl_2$ ligands only at (111), and with $PbCl_2$ attached to both (110) and (111) surfaces. Even in these cases, we observed that 2D NPLs were more favorable compared to 3D structures. Overall, we predict that 2D NPL formation starts with the favorable attachment of $PbCl_2$ ligands at the (110) surface, followed by collision with another QD that leads to formation of a bridge in the (100) direction, loss of amines from the involved (100) surfaces, and finally 2D attachment. This can be repeated in either of the (100) directions to create a 2D structure, but according to our calculations, is not favorable in the direction that remains amine passivated.

As shown in Table S4 and S5, equivalent simulations using the smaller, 1 nm QDs [$(PbSe)_{16}$], produce 2D structures featuring a highly-distorted crystal lattice, which results in higher surface energy as compared to 2D NPL formed from 2 nm $(PbSe)_{68}$ QDs. This suggests there is a critical size of QD for which NPL formation is favored, which is reflected in the lack of any observation of NPLs thinner than 2 nm in experiments.

Table S4: VASP optimized structures of the $(PbSe)_{68}$ and $(PbSe)_{16}$ quantum dot passivated by $PbCl_2$ ligands in either 110 or 111 or both as labelled below:

System	'2D' xy projected along (100)	'2D' yz projected along (100)	'2D' zx projected along (100)	'3D' xyz projected along (111)
$(PbSe)_{68}$ + $(12(PbCl_2))_{110}$	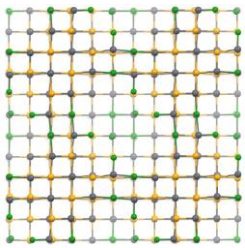	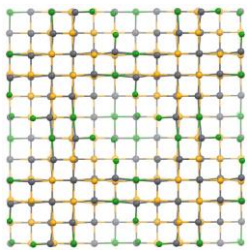	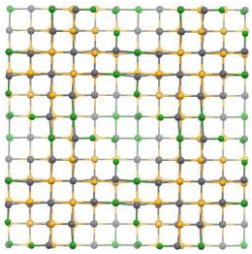	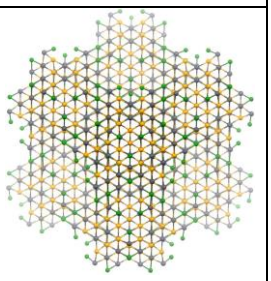
$(PbSe)_{68}$ + $(4(PbCl_2))_{110}$	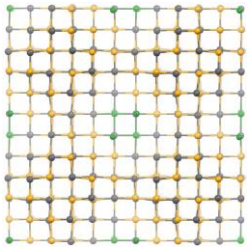	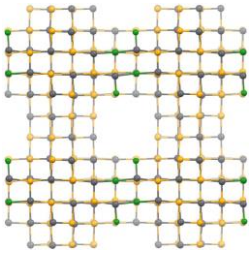	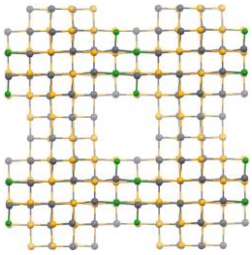	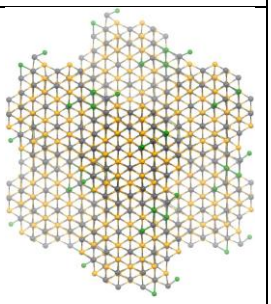
$(PbSe)_{68}$ + $(4(PbCl_2))_{111}$	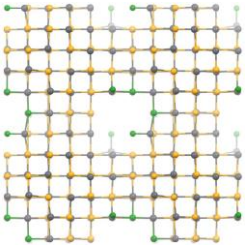	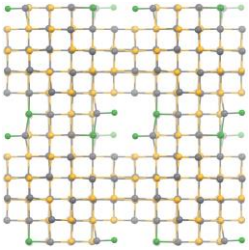	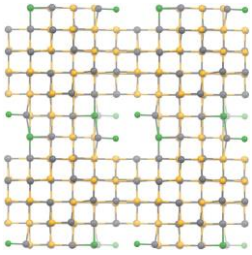	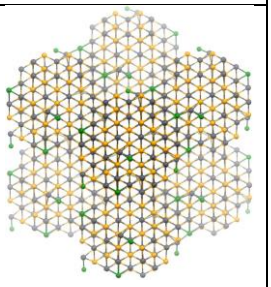
$(PbSe)_{68}$ + $(4(PbCl_2))_{110}$ + $(4(PbCl_2))_{111}$	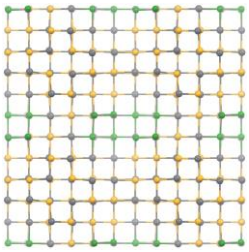	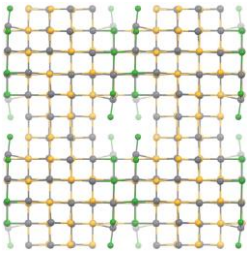	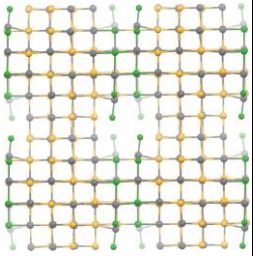	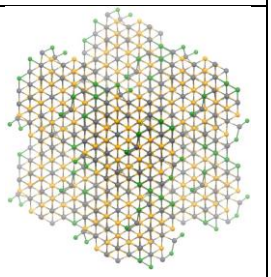

$(PbSe)_{16}$ + $(4(PbCl_2))_{110}$	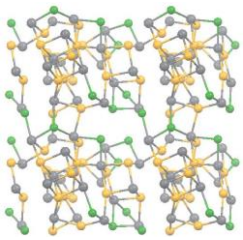	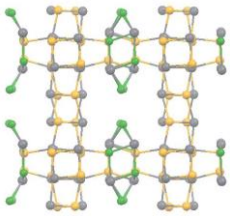	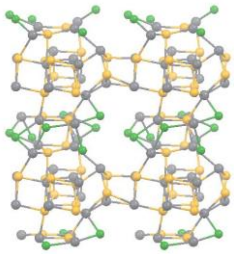	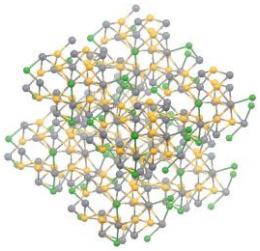

Table S5: Surface energy of the $(PbSe)_{68}$ QD passivated by $PbCl_2$ ligands in either 110 or 111 or both as labelled below, calculated using Eq. 1-11. Values in parenthesis show surface energies for $(PbSe)_{68}$ quantum dot passivated by 12 $PbCl_2$ ligands on 110 surface growing along x- and y-directions, with the z-direction passivated by 6 methyl amines on each (100) side.

System		**$(PbSe)_{68}$/ $12(PbCl_2)_{110}$**	**$(PbSe)_{68}$/ $4(PbCl_2)_{110}$**	**$(PbSe)_{68}$/ $4(PbCl_2)_{111}$**	**$(PbSe)_{68}$/ $4(PbCl_2)_{110}$/ $4(PbCl_2)_{111}$**	**$(PbSe)_{16}$/ $4(PbCl_2)_{110}$**
2D	**xy**	-3.8954 (-4.4574)	-3.9170	-1.3124	-0.9346	-1.0322
	yz	-3.8833 (-4.4575)	-3.9167	-1.3131	-0.9345	-1.0246
	zx	-3.8954 (-4.4572)	-3.9167	-1.3132	-0.9360	-1.02794
3D	**xyz**	-3.7038	-3.7764	-1.0606	-0.7067	-0.9276

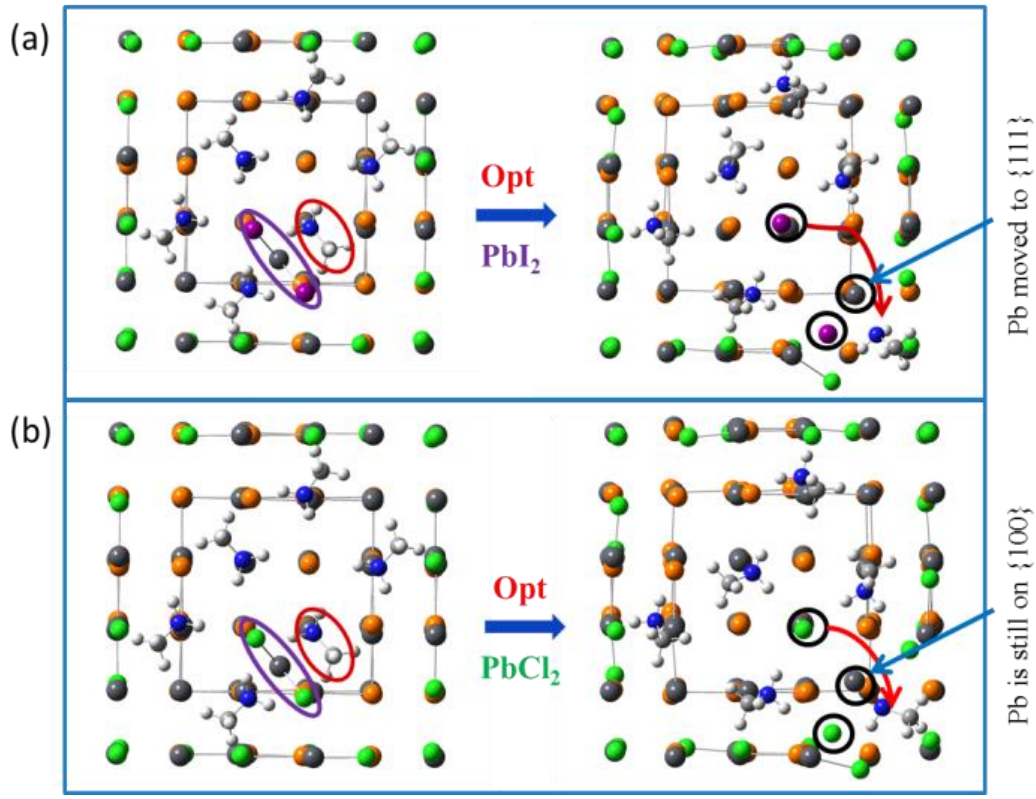

Figure S9: Geometry relaxation of $(PbSe)_{68}$ quantum dot passivated by 12 $PbCl_2$ ligands in either 110, with amines on (100) direction. (a) PbI_2 is placed at (100) and relaxed (b) $PbCl_2$ is placed at (100) and relaxed.

S2.3 Hyperbolic Band Model.

To model the size dependence of the band gap for PbSe NPLs we have extended the hyperbolic band model introduced by Wang and colleagues for the case of a particle in a rectangular box. Within the hyperbolic band model, the band edge transition is treated by only considering the valence and conduction bands which are related via the transfer of an electron from the valence band to the conduction band. A complete derivation of the results has been reported previously.[13] Within this model the size dependent band gap is given by:

$$\Delta E = \left({E_g}^2 + 4\lambda\right)^{1/2} \tag{12}$$

where E_g is the bulk band gap and λ is a morphology dependent term that is found from solving a modified Schrodinger equation for the wavefunction envelope. The resulting terms for a spherical particle and rectangular particle are given by:

$$\lambda_{NC} = {\pi^2 \hbar^2 E_g}/{2m^* R^2} \tag{13}$$

$$\lambda_{NPL} = \frac{\pi^2 \hbar^2 E_g}{2m^*}\left({1}/{L_x{}^2} + {1}/{L_y{}^2} + {1}/{L_z{}^2} \right) \tag{14}$$

Here R is the radius of a spherical NC, L_i is the length of a NPL for i = x, y, or z dimension, and m^* is the effective mass of the carriers, which are assumed to be the same for the conduction and valence band carriers. For the calculations shown figure 4 (c) in the main text the bulk band gap of PbSe was taken to be 0.278 eV, the effective mass $0.077 m_e$, and $L_x = L_y = 18\, nm$ confirmed by atomic force microscopy measurement, which was assumed to be constant while varying the thickness, L_z.

Supporting Information References:

(1) (a) Dai, Q.; Wang, Y.; Li, X.; Zhang, Y.; Pellegrino, D. J.; Zhao, M.; Zou, B.; Seo, J.; Wang, Y.; Yu, W. W. *ACS Nano* **2009**, *3*, 1518; (b) Choi, H.; Ko, J.-H.; Kim, Y.-H.; Jeong, S. *J. Am. Chem. Soc.* **2013**, *135*, 5278; (c) Moreels, I.; Lambert, K.; De Muynck, D.; Vanhaecke, F.; Poelman, D.; Martins, J. C.; Allan, G.; Hens, Z. *Chem. Mater.* **2007**, *19*, 6101.

(2) (a) Kamisaka, H.; Kilina, S. V.; Yamashita, K.; Prezhdo, O. V. *Nano Lett.* **2006**, *6*, 2295; (b) Kilina, S. V.; Craig, C. F.; Kilin, D. S.; Prezhdo, O. V. *J. Phys. Chem. C* **2007**, *111*, 4871; (c) Isborn, C. M.; Kilina, S. V.; Li, X.; Prezhdo, O. V. *J. Phy. Chem. C* **2008**, *112*, 18291; (d) Kamisaka, H.; Kilina, S. V.; Yamashita, K.; Prezhdo, O. V. *J. Phy. Chem. C* **2008**, *112*, 7800; (e) Kilina, S. V.; Kilin, D. S.; Prezhdo, V. V.; Prezhdo, O. V. *J. Phy. Chem. C* **2011**, *115*, 21641; (f) Hedrick, M. M.; Mayo, M. L.; Badaeva, E.; Kilina, S. *J. Phy. Chem. C* **2013**, *117*, 18216.

(3) Frisch, M. J.; Trucks, G. W.; Schlegel, H. B.; Scuseria, G. E.; Robb, M. A.; Cheeseman, J. R.; Scalmani, G.; Barone, V.; Mennucci, B.; Petersson, G. A.; Nakatsuji, H.; Caricato, M.; Li, X.; Hratchian, H. P.; Izmaylov, A. F.; Bloino, J.; Zheng, G.; Sonnenberg, J. L.; Hada, M.; Ehara, M.; Toyota, K.; Fukuda, R.; Hasegawa, J.; Ishida, M.; Nakajima, T.; Honda, Y.; Kitao, O.; Nakai, H.; Vreven, T.; Montgomery, J., J. A.; ; Peralta, J. E.; Ogliaro, F.; Bearpark, M.; Heyd, J. J.; Brothers, E.; Kudin, K. N.; Staroverov, V. N.; Koba-yashi, R.; Normand, J.; Raghavachari, K.; Rendell, A.; Burant, J. C.; Iyengar, S. S.; Tomasi, J.; Cossi, M.; Rega, N.; Millam, N. J.; Klene, M.; Knox, J. E.; Cross, J. B.; Bakken, V.; Adamo, C.; Jaramillo, J.; Gomperts, R.; Stratmann, R. E.; Yazyev, O.; Austin, A. J.; Cammi, R.; Pomelli, C.; Ochterski, J. W.; Martin, R. L.; Morokuma, K.; Zakrzewski, V. G.; Voth, G. A.; Salvador, P.; Dannenberg, J. J.; Dapprich, S.; Daniels, A. D.; Farkas, Ö.; For-esman, J. B.; Ortiz, J. V.; Cioslowski, J.; Fox, D. J. *Gaussian 09*; Gaussian, Inc.: Wallingford CT., 2009.

(4) (a) Perdew, J. P.; Burke, K.; Ernzerhof, M. *Physical review letters* **1996**, *77*, 3865; (b) Ernzerhof, M.; Scuseria, G. E. *J. Chem. Phys.* **1999**, *110*, 5029; (c) Adamo, C.; Barone, V. *J. Chem. Phys.* **1999**, *110*, 6158.

(5) (a) Hay, P. J.; Wadt, W. R. *J. Chem. Phys.* **1985**, *82*, 299; (b) Hay, P. J.; Wadt, W. R. *J. Chem. Phys.* **1985**, *82*, 270; (c) Wadt, W. R.; Hay, P. J. *J. Chem. Phys.* **1985**, *82*, 284.

(6) (a) Francl, M. M.; Pietro, W. J.; Hehre, W. J.; Binkley, J. S.; Gordon, M. S.; DeFrees, D. J.; Pople, J. A. *J. Chem. Phys.* **1982**, *77*, 3654; (b) Hariharan, P. C.; Pople, J. A. *Theoret. Chim. Acta* **1973**, *28*, 213; (c) Hehre, W. J.; Ditchfield, R.; Pople, J. A. *J. Chem. Phys.* **1972**, *56*, 2257.

(7) (a) Cossi, M.; Rega, N.; Scalmani, G.; Barone, V. *J. Comput. Chem.* **2003**, *24*, 669; (b) Barone, V.; Cossi, M.; Tomasi, J. *J. Comput. Chem.* **1998**, *19*, 404.

(8) (a) Kresse, G.; Furthmuller, J. *Comput. Mater. Sci.* **1996**, *6*, 15; (b) Kresse, G.; Furthmüller, J. *Phys. Rev. B* **1996**, *54*, 11169.

(9) Perdew, J. P.; Burke, K.; Ernzerhof, M. *Phys. Rev. Lett.* **1997**, *78*, 1396.

(10) (a) Blöchl, P. E. *Phys. Rev. B* **1994**, *50*, 17953; (b) Kresse, G.; Joubert, D. *Phys. Rev. B* **1999**, *59*, 1758.

(11) Monkhorst, H. J.; Pack, J. D. *Phys. Rev. B* **1976**, *13*, 5188.

(12) Fischer, G.; Poteau, R.; Lachaize, S.; Gerber, I. C. *Langmuir* **2014**, *30*, 11670.

(13) Wang, Y.; Suna, A.; Mahler, W.; Kasowski, R. *J. Chem. Phys.* **1987**, *87*, 7315.